Available online at www.sciencedirect.com
SCIENCE DIRECT
Polymer 46 (2005) 12556–12566
polymer
www.elsevier.com/locate/polymer

# The link between rigid amorphous fraction and crystal perfection in cold-crystallized poly(ethylene terephthalate)

R. Androsch [a,*], B. Wunderlich [b]

[a] Institute of Materials Science, Martin-Luther-University Halle-Wittenberg, D-06099 Halle/S., Germany
[b] Department of Chemistry, University of Tennessee, Knoxville, TN 37996-1600, USA

Received 15 August 2005; received in revised form 13 October 2005; accepted 20 October 2005
Available online 10 November 2005

**Abstract**

The rigid-amorphous fraction (RAF) in cold-crystallized and subsequently annealed poly(ethylene terephthalate) (PET) was investigated as a function of crystallinity and crystal perfection. During cold-crystallization, the amount of RAF increases non-linearly with crystallinity to a maximum of 44% at a crystallinity of 24%. Vitrification of the RAF is almost complete at the cold-crystallization temperature. Increasing the crystallinity from 24% after cold-crystallization to 44% by subsequent annealing at higher temperatures decreases the RAF. The specific RAF, i.e. the ratio of RAF to crystallinity at the glass transition temperature, $T_g$, of the mobile-amorphous fraction decreases from almost 2.0 after cold-crystallization to 0.75 after the subsequent annealing. The decrease in the specific RAF is attributed to crystal perfection which decreases the strain transmitted to the amorphous phase. Analysis of the reversing specific heat capacity of the annealed samples on cooling leads to the conclusion that the remaining RAF at the temperature of annealing is still glassy up to at least 490 K. An observed excess heat capacity above 490 K is due to reversible melting and is discussed within the frame of the concept of the specific reversibility of melting.


*Keywords:* Poly(ethylene terephthalate); Rigid amorphous fraction; RAF

## 1. Introduction

Semi-crystalline, linear polymers consist of a crystalline phase and an amorphous phase, both being connected by tie molecules. The tie-molecule that appears in both phases, thus, is decoupled at the resulting interface and its different segments are described by other values of their functions of state and their physical properties. Because of the geometrical constraints within the phase structure, the decoupling, however, may be incomplete, allowing strain between the phases. The effect of the strain is particularly obvious in the amorphous phase, causing the widely reported broadening of the glass transition to higher temperature in semi-crystalline polymers. In case of sufficiently strong coupling, the affected molecular segments may be sufficiently large, to produce a separate, intermediate phase with a glass transition separated from that of the unaffected amorphous phase. Such observations were made over 20 years ago, and the affected part of the amorphous phase was called a rigid-amorphous fraction, RAF [1,2]. This additional, rigid-amorphous phase, in case of homopolymers, is of the same chemical nature and gains its properties, which are distinct from the amorphous phase, through its interfaces. Since only nanophases are sufficiently small to change their internal properties from the bulk properties due to interactions between the opposing surfaces, the RAF must be a nanophase [3]. This intermediate phase, forming the extended boundary between the crystalline and amorphous phases, was suggested earlier to be characterized by lower, local entropy than that of the fully amorphous phase [4–6]. The intermediate character of the crystal-amorphous interface is furthermore evidenced by a density-difference between the crystalline and amorphous phase of typically 10–15%. A step-like change of the density as function of distance would only be possible in case of complete molecular decoupling of the crystalline and amorphous phases, which, in turn, would require perfect fold-surfaces of the lamellar crystals or an extended-chain crystal morphology. A surface structure with non-adjacent reentry of molecules into the crystal favors an imperfect fold-surface with tie-molecules causing a coupling between the neighboring phases and a gradual change of the density. The locking of molecule segments at the crystal surface reduces the local mobility of chains and results in an increased glass

* Corresponding author. Tel.: +49 3461 46 3762; fax: +49 3461 46 3891.
*E-mail address:* rene.androsch@iw.uni-halle.de (R. Androsch).

0032-3861/$ - see front matter © 2005 Elsevier Ltd. All rights reserved.
doi:10.1016/j.polymer.2005.10.099

transition temperature $T_g$ of the RAF. The consequence is a decreased density of the RAF compared to the mobile amorphous structure at temperatures below the glass transition [7]. The local $T_g$ of the crystal-amorphous interface, therefore, is a measure of the degree of the restriction of cooperative chain-mobility caused by the molecular link to the crystals and is not primarily related to the free volume. On heating, the restrained amorphous structure, which surrounds the crystals, remains rigid at the glass transition of the unrestrained amorphous structure, and is, therefore, often denoted as rigid amorphous-fraction of the amorphous phase, RAF [1,2]. Note that the term rigid amorphous is not related to the actual state of vitrification rather the existence of a restrained amorphous structure with an increased $T_g$. The formation of the RAF is coupled to the crystal formation. For melt-crystallized polycarbonate and poly(3-hydroxy butyrate) it was proven, that the vitrification occurs parallel to the crystal formation [8,9], and for poly(oxy-2,6-dimethyl-1,4-phenylene) it was proven to disappear parallel to melting [10,11]. The exact temperature of vitrification on cooling and devitrification on heating, however, is often difficult to determine, since the glass transition of the RAF is expected to be gradual, according to the gradual change of structure between crystal and unrestrained amorphous phase. Furthermore, at the crystal surfaces there may exist local thermodynamic equilibria which cause crystallization on cooling and melting on heating in equilibrium with temperature [12–14]. Such a local equilibrium is also evidenced for the fold-surface of polyethylene lamellae, which results in a reversible thickening of crystals with temperature, affecting the population of molecule sequences which are part of the rigid amorphous structure.

Quantitative analysis of the glass transition revealed the existence of a RAF for numerous semi-crystalline polymers including polyoxymethylene [1], poly(ethylene terephthalate) [2,7,15–25], poly(trimethylene terephthalate) [26], poly(butylene terephthalate) [27,28], poly(ether ether ketone) [29], polycarbonate [8,9], poly(3-hydroxy butyrate) [8], poly(oxy-2,6-dimethyl-1,4-phenylene) [10,11], poly(phenylene sulfide) [30,31] and polypropylene [8,32]. Recent quantitative analysis of the mechanical relaxation behavior using dynamic mechanical analysis of samples of different crystallinity and crystal morphology demonstrated even in case of polyethylene the stiffening effect of the crystalline phase on the amorphous structure [33], which was proposed earlier on the basis of the broadened thermal glass transition [34].

The RAF in semi-crystalline polymers not only affects the vitrification and devitrification of the amorphous structure, it also has a direct impact on the local melting behavior of crystals [4,14,35,36] and the macroscopic mechanical behavior [37,38]. Therefore, it needs to be characterized for an understanding of the properties of semi-crystalline polymers. The scope of the present study is the further investigation of the amount of RAF and its vitrification/devitrification behavior in poly(ethylene terephthalate) (PET). The PET is an appropriate polymer for analysis of the rigid amorphous phase due to its slow crystallization, which permits to adjust the crystallinity in small increments between zero and close to about 50% [39]. We attempt to establish a link between the RAF on one side, and the crystallinity, crystal size and crystal perfection on the other. In other words, we expect that with increasing crystal perfection, the coupling between crystalline and amorphous structure is reduced, resulting in a decrease in the amount of RAF and the local strain at the crystal surfaces. Since, the RAF is considered to be a measure of the coupling of the crystalline and the amorphous structure, we intend to prove a relation between the occurrence of the RAF and reversible melting. Reversible melting at the surface of crystals is increased if there is strong coupling to the surrounding amorphous structure by covalent bonds, as is evident in small and defective crystals [40,41]. Reversible melting in PET was detected and analyzed since the commercial establishment of temperature-modulated calorimetry [42–44]. It is evidenced that the specific degree of reversibility of melting, i.e. the fraction of molecular sequences which on temperature-modulation crystallize and melt at the surface, depends on the crystallization history. Cold-crystallization, for instance, results in formation of poor crystals which show a larger amount of reversible melting than crystals formed by crystallization from the melt, likely due to the larger specific surface area and increased linkage of crystals and amorphous structure [43].

Systematic analysis of the rigid amorphous phase in PET as function of the inter-lamellar spacing revealed that the thickness of the strained amorphous structure at the surface of lamellae is about 2 nm, being almost independent of the lamellar thickness. It was found that the overall mobility of the amorphous phase increases with increasing crystallization temperature, i.e. the ratio between the rigid and mobile amorphous fractions decreases with increasing crystallization temperature. The temperature of the thermal glass transition increases with ongoing primary crystallization by about 10 K, due to the restriction of mobility at the crystal surfaces, and decreases for samples of identical crystallinity with increasing crystallization temperature. The decrease in the $T_g$ is consistent with the proposed increased mobility of the amorphous structure if crystallization occurred at higher temperature [15–17].

Recent studies focused on oxygen transport/solubility [7] and positron annihilation lifetime spectroscopy [19] in rigid and mobile amorphous PET. The specific free volume of the RAF is reported to be identical to the specific free volume of the melt at the crystallization temperature, and, therefore, higher than the specific free volume of the mobile amorphous fraction. Calorimetric data within the same study revealed furthermore that cold crystallization at 383 K resulted in a maximum degree of crystallinity of 25% with an RAF of 37%. Melt-crystallization at 483 K, in turn, resulted in a degree of crystallinity of 35% and an RAF of only 14%. The large amount of RAF obtained by cold-crystallization was attributed to a larger number of lamellar stacks per crystalline fraction in comparison to melt-crystallized PET.

The above described reports point to a distinct dependence of the nature and fraction of the rigid amorphous phase on the super-molecular structure in PET, which is further investigated in detail within the present study using standard calorimetry,

and temperature-modulated calorimetry with the advantage of increased precision in determination of the temperature-dependence of the heat capacity as the tool for characterization of the RAF.

## 2. Experimental

### 2.1. Materials

A commercial, bottle-grade PET S93 with an intrinsic viscosity of 0.80 dL $g^{-1}$ and a mass-average molecular weight of about 73 kg $mol^{-1}$ [45] provided by the Dow Chemical Company was used for the analysis. The PET was dried before processing to obtain a moisture content of less than 50 ppm. Films of thickness and lateral width of 1 mm × 20 mm were produced by extrusion of the melt into a water-bath, followed by take-up rolls and a wind-up station using a twin-screw extruder ZE 25 from Berstorff. The obtained film was amorphous, as evidenced by X-ray analysis, density, and enthalpy.

### 2.2. Instrumentation

#### 2.2.1. Calorimetry

Calorimetric data were collected with a differential scanning calorimeter DSC 7 from Perkin–Elmer, equipped with the cryonic cooling accessory CCA 7 for operation at sub-ambient temperature and for cooling at controlled rate up to 50 K $min^{-1}$ to ambient temperature. The furnace was purged with nitrogen at a flow rate of 40 mL $min^{-1}$ for minimization of oxidative degradation and for ensuring a reproducible heat-flow path between heater and sample. Circular and flat specimens with a mass of about 8–10 mg were punched from the film and placed in 20 μL aluminum pans from Mettler-Toledo. The calibration of the instrument involved the standard procedure which included a temperature calibration by measurement of the onset of melting of indium, tin, and lead, and an initial heat-flow-rate calibration using the heat of fusion of indium. The raw data of the heat-flow rate were then corrected for instrumental asymmetry by subtraction of a baseline which was measured with empty pans in the sample and reference furnaces under identical instrumental conditions, including matched masses of the aluminum pans within 0.05 mg. The baseline-corrected heat-flow-rate, finally, was converted into apparent specific heat capacity and calibrated using a comparison of the measured and expected heat capacity of sapphire. The rate of temperature change was 20 K $min^{-1}$ in all experiments if not stated otherwise. The selected experimental conditions yield an absolute error of the apparent heat capacity of less than ±3%.

Temperature-modulated differential scanning calorimetry (TMDSC) was performed in the quasi-isothermal mode, using an amplitude and period of modulation of 1.0 K and 120 s, respectively. The heat-flow data were corrected for the instrumental asymmetry by subtraction of a baseline in the time domain, and converted into an apparent reversing specific heat capacity [46]. Parallel measurements were done on a heat-flux differential scanning calorimeter DSC820 (Mettler-Toledo) to exclude inadvertent instrument effects. Calibration and selection of modulation parameters were based on a recent study describing the performance of the particular instrument [47]. Application of TMDSC reduces the absolute error of the apparent heat capacity to ±1%.

#### 2.2.2. Measurement of the RAF by calorimetry

The detection of different mobile-amorphous fractions by thermal analysis is straightforward. In absence of irreversible structural changes and reversible crystallization and melting, differential scanning calorimetry (DSC) yields the thermodynamic specific heat capacity, $c_p$, as a function of temperature $T$. For solids, $c_p$ is practically fully represented by the effect of the vibrational motion. In case of multi-phasic structures, the overall $c_p$ is represented well by the sum of the $c_p$s multiplied with the respective weight-fractions [48]. In case of semi-crystalline polymers with differently mobile amorphous fractions the overall $c_p$ is given by Eq. (1):

$$c_p(T) = m_{cry}(T)c_{p,cry}(T) + m_{am,rigid}(T)c_{p,am,rigid}(T) + m_{am,mobile}(T)c_{p,am,mobile}(T), \quad (1)$$

where $m$ is the mass fraction, and the subscripts 'cry', 'am,rigid', and 'am,mobile' denote crystalline, rigid amorphous, and mobile amorphous. Note, that not only the heat capacities, but also the phase compositions depend on temperature. The temperature dependencies of the heat capacity of the crystalline and amorphous structures are known and listed in the ATHAS Data Bank [49] for a number of polymers, including PET. The heat capacity of the crystalline phase increases steadily with increasing temperature, whereas the temperature-dependence of the amorphous PET shows on heating a step-like increase at the $T_g$ due to the onset of the large-amplitude, cooperative motion characteristic of the liquid [50]. The heat capacity of the glass is identical or close to that of the crystal, and above $T_g$, the heat capacity of the amorphous structure is that of the liquid. The increase in $c_p$ at $T_g$ in absence of crystals is approximately 11 J $K^{-1}$ $mol^{-1}$ of small mobile unit in the liquid and is expected to be linearly reduced with increasing crystallinity if the devitrification of the amorphous glass occurs as a single event:

$$\Delta c_p(T = T_g) \approx (c_{p,liquid} - c_{p,solid})(1 - \text{crystallinity}) \quad (2)$$

$\Delta c_p$ at $T = T_g$ is the relaxation strength of the amorphous phase at $T_g$. The expected $\Delta c_p$ of the decoupled amorphous phase at $T_g$ can, therefore, be estimated, if the crystallinity is known, and is reduced in presence of a restrained RAF.

#### 2.2.3. Density measurement

The density of samples was measured at 296 K with a density gradient column from Ray-Ran using a mixture of water and potassium iodide. The column was prepared such that a density range of 1.32–1.42 g $cm^{-3}$ was covered. The calibration was with glass beads of a defined density, equally distributed along the column. Samples were directly taken from the aluminum pans after the calorimetric analysis, to ensure maximum correspondence between the experiments. From the

measured densities, $\rho$, the weight-fraction crystallinity, $X_{c,\rho}$, was calculated using Eq. (3)

$$X_{c,\rho} = \left(\frac{\rho_c}{\rho}\right)\left[\frac{(\rho-\rho_a)}{(\rho_c-\rho_a)}\right] \quad (3)$$

where $\rho_c$ and $\rho_a$ are the densities of crystalline and amorphous PET, respectively. The density of the amorphous PET is 1.337 g cm$^{-3}$, and the density of crystalline PET is reported to be between 1.338 and 1.578 g cm$^{-3}$, strongly depending on preparation [51]. In the present study a value of 1.498 g cm$^{-3}$ is used, as suggested in [39].

*2.2.4. Wide-angle X-ray scattering*

Wide-angle X-ray scattering data were taken on a diffractometer URD 63 from Seifert-FPM in the transmission mode, using Ni-filtered Cu $K_\alpha$ radiation and a scintillation counter for registration. The X-ray analysis was done on samples which were analyzed before by calorimetry.

## 3. Results and initial discussion

### *3.1. Cold-crystallization*

X-ray-amorphous PET was heated to 390 K and isothermally cold-crystallized for different periods of time. Subsequently, after cold-crystallization, the sample was cooled to 298 K, and reheated to 573 K. The effect of isothermal cold-crystallization for different periods of time at 390 K serves as the controlled adjustment of crystallinity. Fig. 1 shows the density as function of the time of isothermal cold-crystallization. The initial density of the sample is 1.339 g cm$^{-3}$ and is close to the reported value of amorphous PET of 1.337 g cm$^{-3}$, i.e. the initial crystallinity is zero. The density at 296 K after completed cold-crystallization at 390 K is 1.373 g cm$^{-3}$ which can be recalculated into a density-based crystallinity of 24%. Each data point in Fig. 1 represents a separate sample which was subsequently analyzed regarding its glass transition, i.e. the fraction of mobile and rigid-amorphous phases. Fig. 2 is a plot of the heat capacity increment $\Delta c_p$ at the temperature of the glass transition of the mobile amorphous phase as a function of density (filled symbols, bottom axis) and as a function of the enthalpy of fusion (open symbols, top axis). The heat capacity increment was calculated from the heat-capacity data observed on cooling, in order to avoid difficulties in data reduction by superposition of the glass transition with the enthalpy relaxation, which commonly is observed during heating of PET [34,52]. Furthermore, we preferred to analyze the glass transition on cooling since after passing the glass transition on heating the material continued to crystallize, complicating the determination of the heat capacity increment. The heat of fusion was calculated from the final heating scan, taking into account the continued cold-crystallization at temperatures above 390 K. Thus, the heat of fusion is proportional to the degree of crystallinity at $T_g$ of the mobile amorphous fraction. Note that there is close correspondence of the data sets, $\Delta c_p$ versus density (filled symbols, bottom axis), and $\Delta c_p$ versus heat of fusion (open symbols, top axis), respectively, by application of a heat of fusion of fully crystalline PET of 140.1 J g$^{-1}$ [49]. The two dotted vertical lines in Fig. 2 are matches of the density and heat of fusion of fully amorphous and crystalline PET which serve as reference for calculation of the density-based crystallinity and enthalpy-

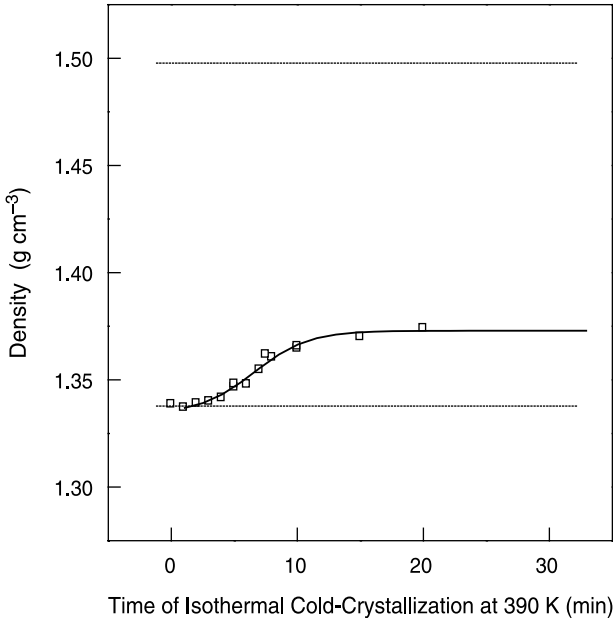


Fig. 1. Density as a function of time of isothermal cold-crystallization at 390 K. The dotted lines represent the density of fully amorphous (1.337 g cm$^{-3}$) and fully crystalline PET (1.498 g cm$^{-3}$).

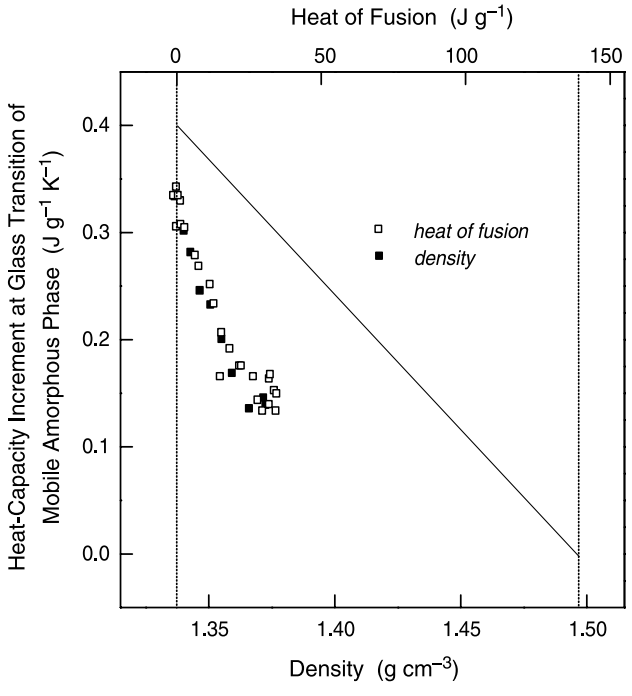


Fig. 2. Heat-capacity increment at the temperature of the glass transition of the mobile-amorphous phase as a function of density (filled symbols, bottom axis) and as a function of enthalpy of fusion (open symbols, top axis). The vertical dotted lines represent the density and heat of fusion of fully amorphous and fully crystalline PET. The solid line represents the expected increment in $c_p$ of the two-phase model.

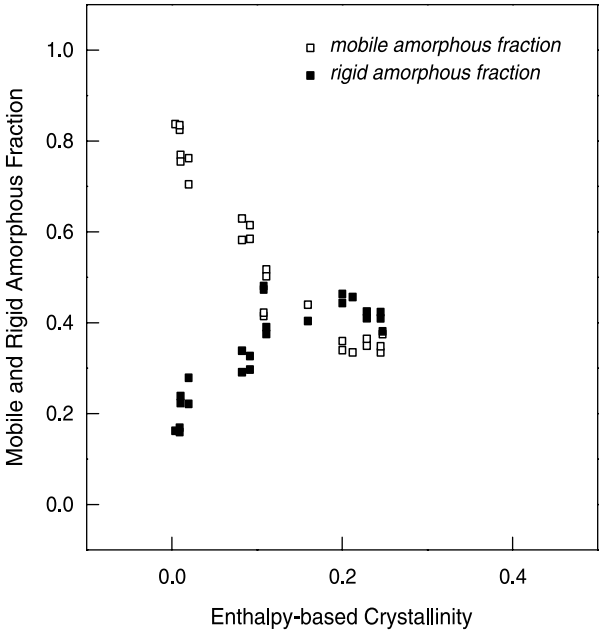


Fig. 3. Mobile amorphous fraction and RAF of PET as function of the enthalpy-based crystallinity, formed during cold-crystallization at 390 K.

based crystallinity. The solid line represents the expected $\Delta c_p$ in case of validity of the two-phase model. The obvious difference between measured data and data representing the two phase-model indicates the presence of a vitrified RAF. Note furthermore that $\Delta c_p$ of the initial non-crystallized sample is $0.34\ J\ g^{-1}\ K^{-1}$ which is less than the expected value listed in the ATHAS data base [49]. The ATHAS data base suggests a heat capacity increment of $0.405\ J\ g^{-1}\ K^{-1}$. Experimental data about the heat capacity increment of amorphous PET are inconsistent, i.e. there are reported values between $0.41\ J\ g^{-1}\ K^{-1}$ [20,21] and $0.33\ g^{-1}\ K^{-1}$ [7,19,22]. A reasonable explanation for the observation of a lowered heat capacity increment in X-ray amorphous PET is the existence of mesomorphic domains which can be considered as precursors for the subsequent crystallization process. These domains cause a stiffening of the structure, and cannot be detected by X-rays due to the small size. Evidence for the existence of heterogeneities in amorphous PET is documented in the literature, using electron microscopy and spectroscopy for detection [51,53].

Fig. 3 is a plot of the rigid and mobile amorphous fractions as a function of the enthalpy-based crystallinity. The initial X-ray amorphous material contains 10–20% rigid amorphous structure of identical density as the mobile amorphous structure. The recently suggested decreased density of the RAF is not confirmed, likely due to insufficient sensitivity of the experiment [7]. The fraction of rigid amorphous phase increases steadily with ongoing crystallization and seems to level off at the final stage of the cold-crystallization process, i.e. the increase in the RAF during crystallization is most pronounced in the early stage of crystallization. After completed cold-crystallization at 390 K the structure composed of approximately 24% crystals, 44% RAF, and 32% mobile amorphous phase, which is similar as was observed in earlier, independent studies [7,15,20,21]. Table 1 is a summary of the crystallinity and the heat-capacity increment at the glass transition of the mobile amorphous structure of cold-crystallized PET, and the calculated phase composition. The table includes data from the present study and data from selected references, and shows the consistency of results despite unavoidable subjectivity in processing of the calorimetric data and the use of different PET grades.

In contrast to the well-investigated phase composition of semi-crystalline PET, there is still uncertainty regarding the temperature of vitrification or devitrification of the RAF on cooling or heating, respectively. The temperature of vitrification on cooling can be estimated by analysis of $c_p$ after completed cold-crystallization at the identical temperature, i.e. at 390 K. The specific heat capacities of amorphous and crystalline PET at 390 K are 1.806 and $1.448\ J\ g^{-1}\ K^{-1}$, respectively. The expected heat-capacity of semi-crystalline PET consisting of 24% crystalline structure and 76% devitrified amorphous structure is, therefore, 1.72 $[\approx 1.806-(1.806-1.448)\times 0.24]$ $J\ g^{-1}\ K^{-1}$. In case of full vitrification of the RAF, the heat capacity would additionally be lowered by 0.16 $[\approx(1.806-1.448)\times 0.44]\ J\ g^{-1}\ K^{-1}$, i.e. the heat capacity would be $1.56\ J\ g^{-1}\ K^{-1}$. Quasi-isothermal analysis of the heat capacity by TMDSC yields a value of $1.63\ J\ g^{-1}\ K^{-1}$ and indicates that vitrification of the rigid amorphous phase only occurs partially at the chosen temperature of the cold-crystallization. Approximately half of the rigid amorphous phase $[(1.63-1.56)/(1.72-1.56)]$ vitrifies on cooling between the temperature of cold-crystallization and the glass transition of the mobile amorphous structure.

### 3.2. Annealing at elevated temperature after cold-crystallization

The second part of the study focuses on the changes of the structure of the cold-crystallized PET on subsequent annealing

Table 1
Heat-capacity increment at the glass transition of the mobile amorphous phase and phase composition of cold-crystallized PET

| Crystallization temperature (K) | Heat-capacity increment ($J\ g^{-1}\ K^{-1}$) | Crystalline fraction | Rigid amorphous fraction | Mobile amorphous fraction | Reference |
|---|---|---|---|---|---|
| 390 | 0.13 | 0.24 | 0.44 | 0.32[a] | This paper |
| 388 | 0.10 | 0.27 | 0.49 | 0.24[a] | 15 |
| 383 | 0.11 | 0.25 | 0.37 | 0.38 | 7 |
| 388 | – | 0.25 | 0.40 | 0.35 | 21 |

[a] Calculated using $0.41\ J\ g^{-1}\ K^{-1}$ as heat-capacity increment of fully amorphous PET.

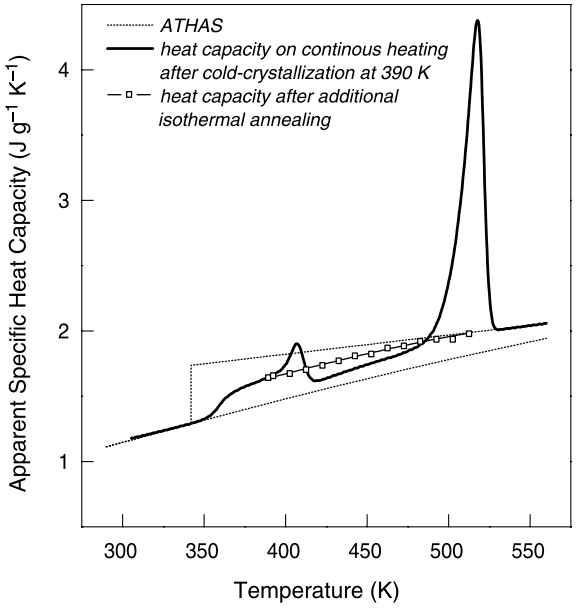


Fig. 4. Apparent specific heat capacity as a function of temperature on melting of PET after cold-crystallization at 390 K for a period of 60 min (solid line). The dotted lines represent the heat capacity of liquid and crystalline PET. The symbols are heat-capacity data obtained after isothermal annealing using TMDSC.

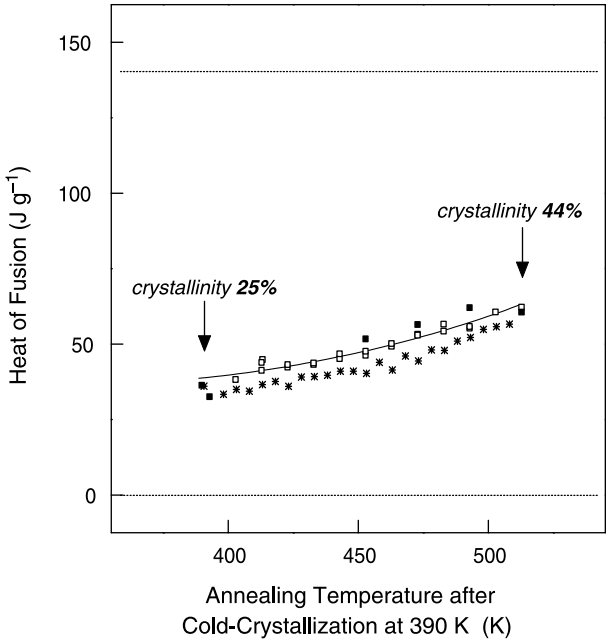


Fig. 5. Heat of fusion as a function of the highest annealing temperature after cold-crystallization of PET. The dotted lines mark the heat of fusion of fully amorphous and crystalline PET. The open and filled squares were obtained after annealing until a metastable state was achieved. The stars represent data obtained by annealing for a period of 10 min.

at higher temperature, and the effect on the fractions and temperatures of vitrification/devitrification, respectively. Annealing was performed at temperatures between 393 and 513 K after cold-crystallization at 390 K for a period of 60 min. Analysis of the glass transition of the annealed samples was done as before using data observed on cooling. The enthalpy-based crystallinity was calculated on melting of the annealed samples. Additional sets of samples were prepared for X-ray analysis and density measurements. Fig. 4 shows with the bold-drawn line the apparent $c_p$ as a function of temperature during continuous heating from 298 to 573 K. The data show the glass transition at about 359 K which is followed by an apparent maximum in $c_p$ at about 407 K, probably related to partial melting of crystals formed at the temperature of cold-crystallization. Further increase in the temperature indicates further cold-crystallization since the apparent $c_p$ is below the, not shown, baseline before final melting starts at about 480 K. The continued irreversible crystallization between the temperature of cold-crystallization and final melting is evidenced on recording of the isothermal change of the apparent $c_p$ on interruption the continuous heating process using TMDSC. Similar data were discussed earlier [43,44] and are, therefore, not shown. The open squares in Fig. 4 represent averages of the apparent $c_p$ for the metastable state, taken at the end of isothermal annealing using the different TMDSC instruments to increase the statistical significance of the data. The difference between the apparent total $c_p$ measured on continuous heating, and the heat capacity after isothermal annealing proves the irreversible arrest of the structure on heating/annealing. During isothermal annealing at higher temperature and further heating, the crystallinity increases and can be quantified by subsequent analysis of the density and heat of fusion.

Fig. 5 is a plot of the heat of fusion after cold-crystallization at 390 K and subsequent annealing as a function of annealing temperature. The open and filled squares were obtained by annealing until structural metastability is reached, again using different calorimeters, and the stars represent data collected after annealing for only 10 min. The crystallinity increases on heating and isothermal annealing from the initial value of 24% after cold-crystallization to 44% after subsequent heating and isothermal annealing at 513 K for a period of 4 h. Furthermore, this treatment increases the perfection of the crystals, as is evidenced by X-ray measurements and inspection of the melting peaks of the annealed samples. The wide-angle X-ray data of Fig. 6 clearly reveal an increase in the intensity of the crystalline scattering due to the increase in the crystallinity. Furthermore, one detects a distinct decrease in the half-width and shift of the position of the crystalline peaks. The change of the peak position as function of the annealing temperature indicates an increase in the crystalline density, and the decrease in the half-width of the crystalline reflections indicates an increased internal order and/or size of crystals. The isothermal annealing after cold-crystallization produces thermodynamically more stable crystals which melt at higher temperatures than the unannealed crystals. These observations are as expected, and are documented in the literature [54–56], and are, therefore, not explicitly shown. Nonetheless, the X-ray data and the analysis of the final melting behavior serve as supporting evidence to establish a semi-quantitative link between the crystallinity and crystal perfection on one side

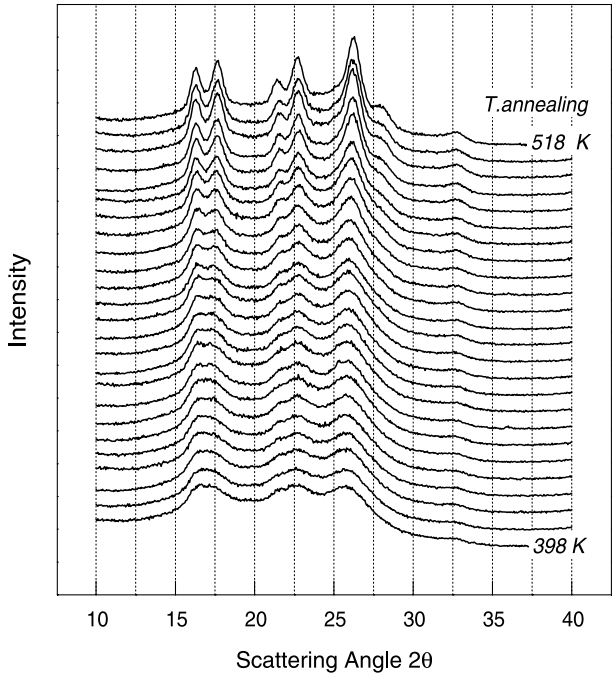


Fig. 6. Wide-angle X-ray data, intensity as function of the scattering angle $2\theta$, of cold-crystallized and subsequently at elevated temperature annealed PET. The annealing temperatures of the bottom and top curve are indicated in the plot, and the increment between two subsequent curves is 5 K.

and the fraction and vitrification behavior of the rigid-amorphous structure on the other side.

Fig. 7 is a plot of the $\Delta c_p$ at $T_g$ of the mobile-amorphous phase as a function of the enthalpy-based crystallinity, controlled by cold-crystallization at 390 K (filled squares) and subsequent annealing at higher temperature (open squares). The solid line is the expected $\Delta c_p$ if the two-phase model would be valid. The $\Delta c_p$ of the cold-crystallized sample decreases as result of the annealing. The decrease in the $\Delta c_p$ from close to 0.14 to almost 0.11 J g$^{-1}$ K$^{-1}$, i.e. by only 0.03 J g$^{-1}$ K$^{-1}$ would correspond to an increase in the crystallinity by less than 8% [=0.03 J g$^{-1}$ K$^{-1}$/0.41 J g$^{-1}$ K$^{-1}$×100%], using 0.41 J g$^{-1}$ K$^{-1}$ as $\Delta c_p$ at vitrification of a fully amorphous sample. The increase in the crystallinity by 20% [=44–24%] in absolute units, however, is 2.5 times the value which would be expected if the change of the heat capacity increment would only be due to the change in crystallinity. The data suggest, therefore, a changed ratio between rigid- and mobile-amorphous fractions as a result of the annealing process. The fractions on mobile and rigid amorphous phases are shown in Fig. 8 as a function of the enthalpy-based crystallinity with the vertical line separating data points observed on cold-crystallization at 390 K (left) and on additional annealing at elevated temperature (right). The data clearly reveal a decrease in the total amount on rigid amorphous phase as result of longer cold-crystallization time and on further annealing at higher temperature. The increase in the crystallinity occurs on expense of both, mobile and rigid amorphous phases. The ratio between rigid amorphous phase to crystalline phase, i.e. the specific RAF, decreases from 44/24 [=1.83] at low crystallinity after completed cold-crystallization at 390 K to 33/44 [=0.75] after additional annealing at 513 K. The average fraction on rigid amorphous structure per crystal is drastically reduced to half its original value, which must be caused by specific changes of the crystal morphology after annealing.

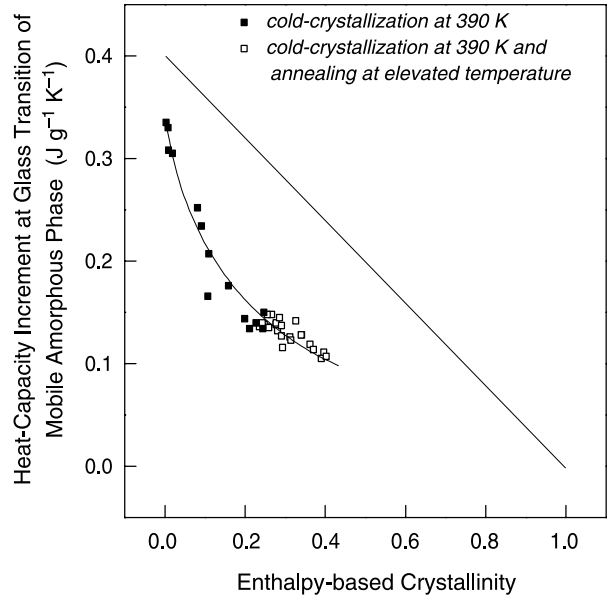


Fig. 7. Heat-capacity increments at the temperature of the glass transition of the mobile amorphous phase as a function of the enthalpy-based crystallinity. The plot includes data obtained on cold-crystallization at 390 K (filled squares), and data obtained after additional annealing at elevated temperature (open squares). The solid line represents the expected heat-capacity increment for the two-phase model.

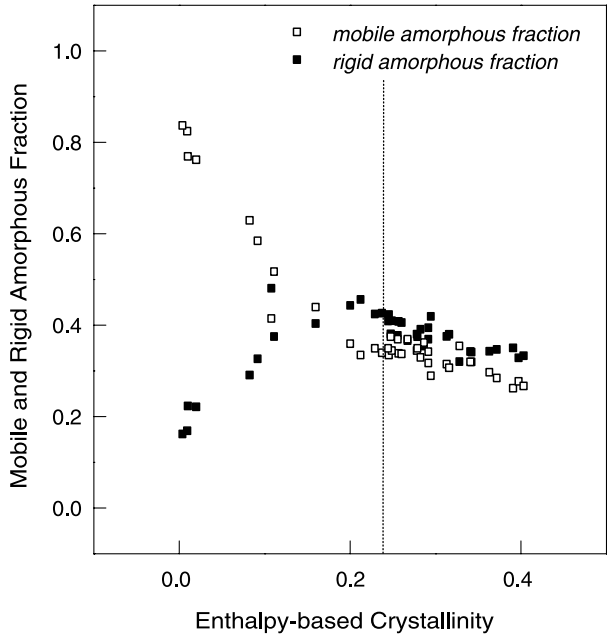


Fig. 8. Mobile amorphous fraction and RAF of PET as a function of the enthalpy-based crystallinity. The vertical line at a crystallinity of 24% separates data points obtained by cold-crystallization at 390 K as function of time, and data points obtained by additional annealing at elevated temperatures.

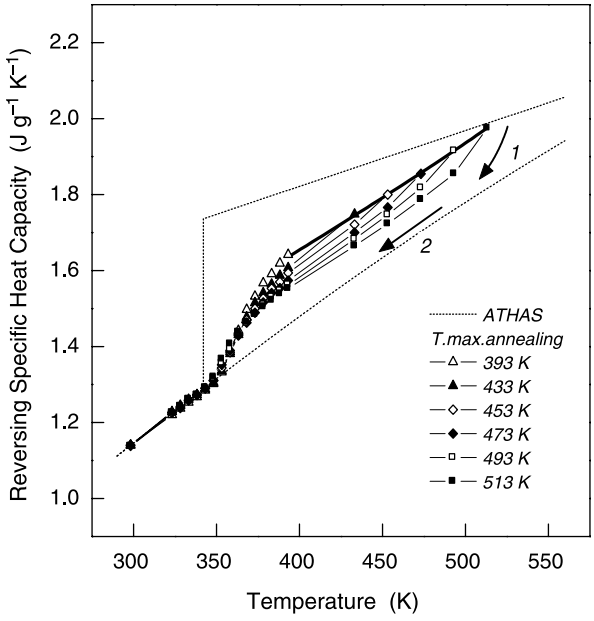


Fig. 9. Reversing $c_p$ of cold-crystallized and subsequently annealed PET at elevated temperatures as a function of temperature. Data were obtained on stepwise cooling with each experiment starting at a different maximum annealing temperature. Heat-capacity data were taken at the end of each quasi-isothermal annealing step with the structure being in metastable thermodynamic equilibrium.

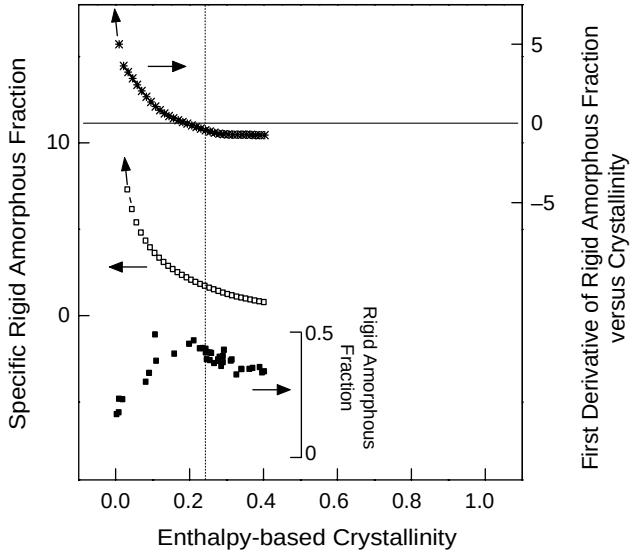


Fig. 10. The RAF of PET (filled squares, inset axis), specific RAF (open squares, left axis), and the first derivative of RAF versus crystallinity (stars, right axis) as a function of the enthalpy-based crystallinity. The vertical line at a crystallinity of 24% separates data points obtained by isothermal cold-crystallization at 390 K, and data points obtained by additional annealing at elevated temperatures. The horizontal line is related to the right axis for illustrating the zero-crossing of the first derivative of the RAF.

Fig. 9 shows the reversing apparent $c_p$ of cold-crystallized PET, which was subsequently annealed at higher temperature, followed by additional annealing at stepwise lowered temperatures. The maximum annealing temperature in the different experiments is indicated in the legend. To guide the eye, the data at the maximum annealing temperatures are connected by the heavy solid line. In general, the specific reversing $c_p$ decreases in the stepwise cooling after annealing. This decrease in $c_p$ is most pronounced 0–20 K below the maximum annealing temperature, as is indicated by the curved arrow '1' for the maximum annealing temperature of 513 K. The further decrease in $c_p$ down to $T_g$ of the mobile amorphous phase is small relative to the calculated ATHAS data for a fixed phase composition, as is indicated by the arrow labeled '2'. This temperature-dependence of the reversing $c_p$ on cooling after annealing indicates either increasing vitrification of the rigid amorphous phase or decreasing reversible melting. A better separation of these two possible causes is perhaps possible by frequency-dependent analysis of the reversing $c_p$, which, however, requires special instrumentation, not available for the present study [8,9]. Visual inspection of the raw data used in Fig. 9 can identify reversible melting only for the samples initially annealed at 513 and 493 K. This reversible melting, however, was obvious only at the initial, highest temperatures as a larger heat-flow rate, resulting in an excess $c_p$ above the thermodynamic baseline.

## 4. Final discussion and conclusions

The present study focuses on the analysis of the fraction and vitrification/devitrification of the rigid amorphous phase of cold-crystallized and subsequently annealed PET. The RAF is estimated from the heat-capacity increment at $T_g$ of the mobile amorphous phase, and the crystallinity is determined by the heat of fusion and by measurement of the density. The fraction of RAF is shown as a function of crystallinity with the filled squares in Fig. 8, and was reprocessed to a specific RAF which is the RAF divided by crystallinity. The specific RAF can be considered as average amount of rigid amorphous structure per unit of crystal, and is shown in Fig. 10 as function of crystallinity with the open squares (left axis). Furthermore, the first derivative of the RAF versus crystallinity (stars, right axis) is shown in Fig. 10 which clarifies the actual evolution of RAF on increasing the crystallinity. The crystallinity-dependence of the RAF of Fig. 8 (filled squares) is included in Fig. 10 (inset axis) for easy comparison. The vertical line in Fig. 10 separates data obtained on isothermal cold-crystallization (left) from data obtained by subsequent annealing (right), as also shown in Fig. 8.

The RAF increases during isothermal cold-crystallization and reaches a maximum value of 44% at a crystallinity of 24%. Further increase in the crystallinity by subsequent annealing at elevated temperature results in a reduction of the RAF. The specific RAF is largest in the beginning of the crystallization and decreases continuously during the crystallization, apparently independent whether the crystallization occurred isothermally from the glassy state, or on subsequent annealing. At the beginning of the crystallization the specific RAF is $>5$, i.e. the RAF is many times larger than the crystalline fraction. The relative ratio between RAF and crystalline fraction reduces to about 1.7–1.8 after cold-crystallization at a crystallinity of 24%, and decreases further to about 0.7–0.8 after reaching the

maximum crystallinity of 44% by subsequent annealing at 513 K.

We assume that on quenching, as result of large supercooling a large number of nuclei develops, which can be considered as small domains of aligned chain segments with the molecules entering the nucleus at the basal planes, without folding-back themselves to reenter within a tight loop. The existence of nodules of diameter of 4.5–10 nm in quenched PET is evidenced by microscopy [51,53,57] and, perhaps, is detected by the lowered heat-capacity increment in the present study. The molecule segments at the basal planes are conformationally restricted, and cause a large RAF. Reheating quenched PET to the temperature of isothermal cold-crystallization triggers growth and aggregation of the existing nuclei. Growth in longitudinal direction is limited by the constant low temperature of crystallization of 390 K, and occurs, therefore, preferred in lateral direction. The decrease in the specific RAF must, therefore, be explained with a change of the average structure of the basal crystal surfaces since the ratio between the total area of basal planes and crystal volume does not change on crystal growth in lateral direction. We conclude that during the process of cold-crystallization, occasional formation of folds occurs as major source for decoupling of the crystalline and amorphous phases. Folding increases decoupling of crystalline and amorphous phases, and decreases, therefore, the specific RAF. This argument is strongly supported by the crystallinity-dependence of the first derivative of the RAF which clearly evidences that in the late stage of the isothermal cold-crystallization the increase in the crystallinity is not connected with formation of rigid amorphous structure. The increase in the RAF per increase in the crystallinity by 1% is $>5\%$ in the beginning of the cold-crystallization process, whereas, at the end of the cold-crystallization process no RAF develops on increasing the crystalline fraction. The change of formation of RAF with crystallinity or crystallization history, respectively, is not investigated in detail for other polymers which are able to produce a RAF. Different polymers and different crystallization paths will affect the amount of RAF produced on crystallization.

The formation of RAF and crystals is completely changed by annealing. During the approach of the annealing temperature, i.e. on heating, the initially small and disordered crystals formed at 390 K melt at slightly higher temperature (Fig. 4). Simultaneously, recrystallization occurs with the formation of crystals of increased thickness and perfection in accord with the increased crystallization temperature. The increased thickness and perfection of the new or reformed crystals, respectively, can directly be seen by the increased melting temperature which, according to the Turnbull-Fisher-equation, is a direct measure of the thermodynamic stability. Further evidence of the increased crystal size and perfection as result of annealing of PET at elevated temperature is given with the drastic decrease in the half-width of the wide-angle X-ray reflections (Fig. 6). For PET, even of high crystallinity, quick heating to above 500 K leads to increasing melting, reaching completion by about 520 K. This melting is followed by fast recrystallization [58]. In addition, on a slower time-scale, in the presence of moisture at lower temperature, and accelerated at all temperatures by catalysts left from the synthesis, increasing amounts of *trans*-esterification can occur, reducing the number of strained, non-crystalline molecule segments. These effects also were studied earlier and could remove all folds by hydrolysis, to produce oligomer crystals [59]. These oligomer crystals could be reconnected by heating below the melting temperature to high molar mass structures of high melting temperatures [60]. The same mechanism is active on industrially increasing the molar mass and melting temperature by 'solid-state polymerization'.

An attempt to access the temperature of vitrification of the rigid amorphous phase after annealing at elevated temperature is possible from the reversing $c_p$ observed on stepwise cooling and annealing (Fig. 9). These data were recalculated to an excess $c_p$ by subtraction of an appropriate baseline. This baseline depends on crystallinity, which is a function of the highest annealing temperature illustrated in Fig. 5, and which, on subsequent cooling, does not change significantly. The baseline also depends on the state of vitrification of the RAF, which, a priori, is not known. For the sake of discussion, we assumed first that the rigid amorphous structure is fully devitrified over the entire temperature range of analysis. Fig. 11 illustrates this case. It confirms the decrease in the excess $c_p$ on cooling for all data sets, as is seen already in the raw data of Fig. 9 as arrow '1'. The horizontal line in Fig. 11 separates positive and negative excess $c_p$. The vertical position of this line is controlled by the assumed state of vitrification of the RAF. The data of Fig. 11, however, demonstrate impressively that the assumption of complete devitrification of the RAF cannot be true, since a negative reversing excess $c_p$ is impossible. The initial assumption, thus, must be modified.

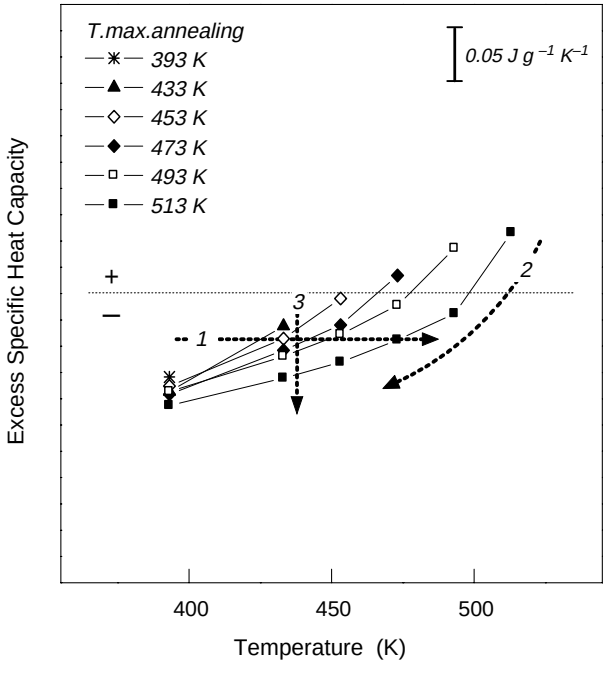


Fig. 11. Excess $c_p$ as a function of temperature. The excess $c_p$ was calculated from the data shown in Fig. 9 as difference between measured reversing $c_p$ and baseline $c_p$.

Vitrification of the rigid amorphous phase must occur either at the temperature of crystallization, i.e. the highest annealing temperature for each experiment, or on subsequent cooling. Vitrification on cooling along the path which is indicated by the curved arrow '1' in Fig. 9 or '2' in Fig. 11 can be ruled out, since in this case the $T_g$ of the rigid amorphous phase would depend on the highest annealing temperature (see horizontal arrow '1' in Fig. 11). An increase in the $T_g$ of the rigid amorphous phase with increasingly higher annealing temperature cannot be true since this would contradict the observation of a decreased average specific RAF after annealing at high temperature in Fig. 10. Therefore, we conclude that vitrification of the rigid amorphous structure occurs mainly at the crystallization temperature or highest annealing temperature, i.e. at the temperature of final establishment of the crystal size, shape, and perfection. This conclusion implies that the temperature-dependence of the excess heat capacity observed on stepwise cooling after annealing is entirely due to reversible melting. The degree of reversible melting is largest at the temperature of annealing and decays on lowering the temperature as marked by arrow '2' in Fig. 11. The temperature dependence of the excess $c_p$, caused by reversible melting, can be explained based on the recently established concept of the specific reversibility of melting [61,62]. This concept predicts a direct relationship between the irreversible change of crystallinity and degree of reversible melting at any given temperature. In other words, if the irreversible crystallinity-increase in annealing on stepwise cooling decreases, then we expect the reversible melting also to decrease at the same temperature. Different crystals contribute to the reversible melting at different temperatures, in this case, annealing temperatures. This argument also would explain the decreasing excess $c_p$ for the different data sets along arrow '3' in Fig. 11. Annealing at high temperature reduces subsequent irreversible crystallization at lower temperature, or, in other words, if the maximum annealing temperature is relatively low, then subsequent isothermal annealing at lower temperatures results in larger irreversible increases in crystallinity. Since we did not detect, however, a major increase in the crystallinity on cooling after annealing at elevated temperature, we also may consider an inherently reduced activity of irreversibility at higher temperature, i.e. for the highest annealing temperature formed or reorganized crystals on decreasing the temperature. This inherent temperature-dependence of reversible melting of a given crystal is not investigated yet, but in semi-crystalline PET it may partly be controlled by the RAF at the crystal boundaries. Nonetheless, we cannot unambiguously prove a relation between the degree of reversible melting and the RAF. We could argue that the observed decreased degree of reversible melting on decreasing the highest annealing temperature (Figs. 9 and 11) is due to an increased specific RAF (Fig. 10). This correlation lacks evidence since it is not known if the reversible melting event involves molecule segments which are part of the rigid amorphous phase. The data rather suggest different populations of molecular segments since reversible melting requires mobility, not possible in a vitrified rigid amorphous structure.

## References


[1] Suzuki H, Grebowicz J, Wunderlich B. Br Polym J 1985;17:1–3.
[2] Menczel J, Wunderlich B. J Polym Sci, Polym Lett 1981;19:261–4.
[3] Chen W, Wunderlich B. Macromol Chem Phys 1999;200:283–311.
[4] Zachmann HG. Kolloid-Z u Z Polymere 1967;216–217:180–91.
[5] Fischer EW. Kolloid-Z u Z Polymere 1967;218:97–104.
[6] Kilian HG. Kolloid-Z u Z Polymere 1967;231:534–64.
[7] Lin J, Shenogin S, Nazarenko S. Polymer 2002;43:4733–43.
[8] Schick C, Wurm A, Mohammed A. Thermochim Acta 2002;392-393: 303–13.
[9] Schick C, Wurm A, Merzlyakov M, Minakov A, Marand H. J Therm Anal Cal 2001;64:549–55.
[10] Cheng SZD, Wunderlich B. Macromolecules 1987;20:1630–7.
[11] Pak J, Pyda M, Wunderlich B. Macromolecules 2003;36:495–9.
[12] Fischer EW. Kolloid-Z u Z Polymere 1967;218:97.
[13] Strobl G, Schneider M, Voigt-Martin I. J Polym Sci, Polym Phys 1980;18: 1361.
[14] Wunderlich B. Progr Polym Sci 2003;28:383–450.
[15] Schick C, Krämer L, Mischok W. Acta Polym 1985;36:47–53.
[16] Schick C, Fabry F, Schnell U, Stoll G, Deutschbein L, Mischok W. Acta Polym 1988;39:705–10.
[17] Schick C, Wigger J, Mischok W. Acta Polym 1990;41:137–42.
[18] Alvarez C, Sics I, Nogales A, Denchev Z, Funari SS, Ezquerra TA. Polymer 2004;45:3953–9.
[19] Olson BG, Lin J, Nazarenko S, Jamieson AM. Macromolecules 2003;36: 7618–23.
[20] Okazaki I, Wunderlich B. J Polym Sci, Polym Symp 1996;34:2941–52.
[21] Zhao J, Dong W, Li C, Guo M, Fan Q. Macromolecules 2003;36:2176–8.
[22] Alves NM, Mano JF, Balaguer E, Meseguer Duenas JM, Gomez Ribelles JL. Polymer 2002;43:4111–22.
[23] Ivanov DA, Pop T, Yoon DY, Jonas AM. Macromolecules 2002;35: 9813–8.
[24] Diego JA, Canadas JC, Mudarra M, Belana J. Polymer 1999;40:5355–63.
[25] Song M, Hourston DJ. J Therm Anal 1998;54:651–7.
[26] Pyda M, Wunderlich B. J Polym Sci, Polym Phys 2000;38:622–31.
[27] Cheng SZD, Pan R, Wunderlich B. Makromol Chem 1988;189:2443–58.
[28] Pyda M, Nowak-Pyda E, Mays J, Wunderlich B. J Polym Sci, Polym Phys 2004;42:4401–11.
[29] Cheng SZD, Cao MY, Wunderlich B. Macromolecules 1986;19:1868–76.
[30] Cheng SZD, Wu ZQ, Wunderlich B. Macromolecules 1987;20:2802–10.
[31] Huo P, Cebe P. J Polym Sci, Polym Phys 1992;30:239–50.
[32] Grebowicz J, Lau SF, Wunderlich B. J Polym Sci, Polym Symp 1984;71: 19–37.
[33] Kolesov IS, Androsch R, Radusch H-J. Macromolecules 2005;38:445–53.
[34] Wunderlich B. Thermal analysis. Boston: Academic Press; 1990.
[35] Wunderlich B. Macromolecular physics. Crystal melting. vol. 3. New York: Academic Press; 1980.
[36] Righetti MC, Di Lorenzo ML, Angiuli M, Tombari E. Macromolecules 2004;37:9027–33.
[37] Rastogi R, Vellinga WP, Rastogi S, Schick C, Meijer HEH. J Polym Sci, Polym Phys 2004;42:2092–106.
[38] Fu Y, Annis B, Boller A, Jin Y, Wunderlich B. J Polym Sci, Polym Phys 1994;32:2289–306.
[39] Kilian HG, Halboth H, Jenckel E. Kolloid-Zeitschrift 1960;172:166–77.
[40] Wu W, Albrecht T, Strobl G. Macromolecules 1999;32:7548–54.
[41] Androsch R, Wunderlich B. Macromolecules 2000;33:9076–89.
[42] Reading M, Hahn BK, Crowe BS. US Patent, Method and apparatus for modulated differential analysis, 5,224,775; July 6, 1993.
[43] Okazaki I, Wunderlich B. Macromolecules 1997;30:1758–64.
[44] Schick C, Merzlyakov M, Wunderlich B. Polym Bull 1998;40:297–303.
[45] Private communication, Koehlmann D, Equipolymers, Germany; 2005.
[46] Androsch R, Moon I, Kreitmeier S, Wunderlich B. Thermochim Acta 2000;357–358:267–78.
[47] Androsch R. J Therm Anal Cal 2000;61:75–89.
[48] Dole M. Fortschr Hochpol Forschung 1960;2:221–74.

[49] Wunderlich B. Pure Appl Chem 1995;67:1019–26.ATHAS Data Bank, http://web.utk.edu/~athas/databank/, Pyda M, editor; 1994.
[50] Wunderlich B. Thermochim Acta 1997;300:43–65.
[51] Geil PH. In: Fakirov S, editor. Handbook of thermoplastic polyesters, vol. 1. Weinheim: Wiley-VCH; 2002.
[52] Montserrat S, Cortes P. Makromol Chem, Macromol Symp 1988;20/21: 389–95.
[53] Yeh GSY, Geil PH. J Macromol Sci Phys 1967;B1:235–50.
[54] Fakirov S, Fischer EW, Schmidt GF. Makromol Chem 1975;176: 2459–65.
[55] Ruscher C, Seganow I, Teichgräber M. Faserforschung und Textiltechnik 1974;25:544–51.
[56] Groeninckx G, Reynaers H. J Polym Sci, Polym Phys 1980;18:1325–41.
[57] Wunderlich B. Macromolecular physics. Crystal nucleation, growth, annealing. vol. 2. New York: Academic Press; 1976.
[58] Zachmann HG, Stuart HA. Makromol Chem 1960;52:23.
[59] Miyagi A, Wunderlich B. J Polym Sci, Polym Phys 1972;10:2073.
[60] Miyagi A, Wunderlich B. J Polym Sci, Polym Phys 1972;10:2085.
[61] Androsch R, Wunderlich B. J Polym Sci, Polym Phys 2003;41:2039–51.
[62] Androsch R, Wunderlich B. J Polym Sci, Polym Phys 2003;41:2157–73.